ACS APPLIED MATERIALS & INTERFACES

www.acsami.org

Research Article

Advancing Human-Centric LED Lighting Using $Na_2MgPO_4F:Eu^{2+}$

Shruti Hariyani and Jakoah Brgoch*

Cite This: *ACS Appl. Mater. Interfaces* 2021, 13, 16669−16676

Read Online

ACCESS | Metrics & More | Article Recommendations | Supporting Information

ABSTRACT: The proliferation of energy-efficient light-emitting diode (LED) lighting has resulted in continued exposure to blue light, which has been linked to cataract formation, circadian disruption, and mood disorders. Blue light can be readily minimized in pursuit of "human-centric" lighting using a violet LED chip ($\lambda_{em} \approx 405$ nm) downconverted by red, green, and blue-emitting phosphors. However, few phosphors efficiently convert violet light to blue light. This work reports a new phosphor that meets this demand. $Na_2MgPO_4F:Eu^{2+}$ can be excited by a violet LED yielding an efficient, bright blue emission. The material also shows zero thermal quenching and has outstanding chromatic stability. The chemical robustness of the phosphor was also confirmed through prolonged exposure to water and high temperatures. A prototype device using a 405 nm LED, $Na_2MgPO_4F:Eu^{2+}$, and a green and red-emitting phosphor produces a warm white light with a higher color rendering index than a commercially purchased LED light bulb while significantly reducing the blue component. These results demonstrate the capability of $Na_2MgPO_4F:Eu^{2+}$ as a next-generation phosphor capable of advancing human-centric lighting.

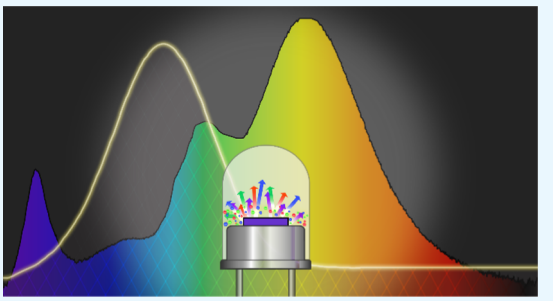

KEYWORDS: *phosphors, oxyfluoride, violet light excitation, luminous efficacy, blue-emitting, melatonin suppression*

1. INTRODUCTION

The concept of human-centric lighting stems from the evolution of sunlight's intensity and correlated color temperature (CCT) throughout the course of a day. This natural progression of bright cold white light during the middle of the day to a softer warm white light in the evening stimulates intrinsic photosensitive retinal ganglion cells that control our circadian rhythm.[1] These cells are activated by the blue-hue of daylight to produce dopamine and cortisol while suppressing melatonin, the sleep hormone, to keep humans awake and alert.[2] The current generation of energy-efficient light-emitting diode (LED) lights reproduce daylight (CCT > 4500 K) by converting the blue emission from an InGaN LED chip ($\lambda_{em} \approx 450$ nm) to a broad spectrum white light using the yellow-emitting $Y_3Al_5O_{12}:Ce^{3+}$ phosphor, illustrated by the spectrum in Figure 1a.[3] The blue LED emission also overlaps with the maximum of the wavelength-dependent melatonin suppression curve (Figure 1a, gray dashed), which, combined with the high CCT, makes it ideal for increasing concentration and stamina during the daytime.[4] LED bulbs can be tuned to warm white light (CCT ≈ 2700 K), as required for nighttime lighting, by adding a second red-emitting phosphor such as $Sr_2Si_5N_8:Eu^{2+}$ shown in Figure 1b; however, the prevalence of the blue emission from the LED remains.[5,6] The resulting chronic blue light exposure has been shown to cause macular degeneration, cataract formation, mood disorders, and circadian disruption, resulting in insomnia and fatigue.[7,8] Therefore, the production of a human-centric warm white light for nighttime use depends on minimizing blue light in LED bulbs.

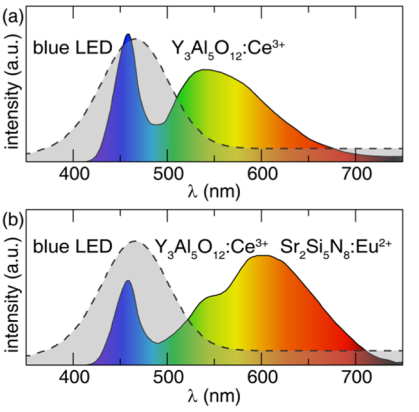

Figure 1. (a) Cold white light generated by combining a blue LED and yellow-emitting $Y_3Al_5O_{12}:Ce^{3+}$ overlaps significantly with a wavelength-dependent melatonin curve (gray, dashed), making it ideal for daytime lighting. (b) Addition of red-emitting $Sr_2Si_5N_8:Eu^{2+}$ produces a warmer white light, but the prevalent blue LED emission remains and can inhibit melatonin production.

Received: January 14, 2021
Accepted: March 22, 2021
Published: March 31, 2021

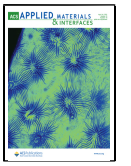

Reducing the intensity of blue light from the LED chip can be achieved using a violet LED chip ($\lambda_{em} \approx 405$ nm) with red, green, and blue-emitting phosphors. White light produced from violet LEDs has additional benefits, including a higher color rendering index (CRI) and luminous efficacy and a lower probability of droop than traditional blue LEDs.[9] This approach also allows for full coverage of the near-UV to the blue region for a continuous spectrum and the formation of a wider color gamut for greater color tunability and selectivity.[10] However, the main consequence of using a violet LED is that the phosphors must have a high photoluminescent quantum yield (PLQY) under 405 nm excitation to overcome the inherent Stokes' loss.[11] Moreover, the phosphors must resist a loss in emission intensity and chromaticity drift as a function of temperature to ensure an unwavering emission color when observed by the average human eye.[12]

There are currently many red and green-emitting phosphors that satisfy all of these requirements. However, most blue-emitting materials reported in the literature cannot be excited by violet light.[4,6,13,14] The most popular blue emitter is arguably $BaMgAl_{10}O_{17}:Eu^{2+}$ ($BAM:Eu^{2+}$). This material has been used in domestic lighting and plasma display-based technologies due to its high PLQY upon excitation with UV ($\lambda_{ex} = 365$ nm; PLQY $\approx$ 99%) and violet ($\lambda_{ex} = 400$ nm; PLQY = 90%) light, following years of optimization.[15] The main drawback is that $BAM:Eu^{2+}$ can be readily hydrolyzed and the rare-earth ion oxidized from Eu^{2+} to Eu^{3+}. This results in noticeable shifts in the emission wavelength and decreased emission intensity upon prolonged operation.[16,17] There are other blue-emitting phosphors with strong absorption in the violet region such as $Sr_3MgSi_2O_8:Eu^{2+}$ and $Ca_5(PO_4)_3Cl:Eu^{2+}$, but these phosphors suffer from poor thermal stability and efficiency, respectively.[18,19] There are few efficient blue-emitting phosphors under 400 nm excitation. $SrLu_2O_4:Ce^{3+}$ (PLQY = 76%) and $Ba_9Sc_2Si_6O_{24}:Ce^{3+}$ (PLQY = 57%) have both been evaluated, although the cost of Lu and Sc make industrial-scale production of these materials cost-prohibitive.[20,21] It is more common to have efficient cyan emission under violet light excitation, like in $RbNa_3(Li_3SiO_4)_4:Eu^{2+}$ and $YScSi_4N_6C:Ce^{3+}$;[22−26] however, cyan light ($\lambda_{em} \approx 480-520$ nm) overlaps with the center of the wavelength-dependent melatonin suppression curve (λ_{max} = 484 nm), where melatonin suppression is maximized.[7,27]

Herein, we report a new violet excited, blue-emitting fluorophosphate phosphor, $Na_2MgPO_4F:Eu^{2+}$. The compound can be synthesized through one-step sintering of naturally abundant precursors. Most importantly, the phosphor possesses a highly efficient, thermally stable blue emission when excited with violet light. The chemical and thermal stability of $(Na_{1.92}Eu_{0.04})MgPO_4F$ was also confirmed through prolonged exposure to water and high temperatures. Finally, a prototype device driven by a 405 nm LED employing $(Na_{1.92}Eu_{0.04})$-$MgPO_4F$ generates a full-spectrum warm white light. There is a considerable reduction of blue light produced by the device while maintaining excellent color rendering. In combination, these results express the suitability and potential for $Na_2MgPO_4F:Eu^{2+}$ in violet LED devices to produce a warm white light that is optimal for humans.

2. METHODOLOGY

2.1. Material Synthesis, Optical Characterization, and Prototype Development. $(Na_{2-2x}Eu_x)MgPO_4F$ (x = 0, 0.005, 0.01, 0.02, 0.04, and 0.06) was prepared via solid-state reaction starting from Na_2CO_3 (Sigma-Aldrich, 99.95%), MgO (Sigma-Aldrich, 99.995%), $NH_4H_2PO_4$ (Acros Organics, 99.9%), MgF_2 (Sigma-Aldrich, 99.99%), and Eu_2O_3 (Alfa Aesar, 99.99%) in the appropriate stoichiometric ratios. An additional 7.5 wt % of Na_2CO_3 was added to compensate for evaporation during synthesis. The starting reagents were initially ground in an acetone medium using an agate mortar and pestle and then further ground for 100 min with a high-energy ball mill (Spex 800 M Mixer/Mill). The powder was then pressed into a 6 mm diameter pellet, placed on a bed of sacrificial powder in an alumina crucible (AdValue Technology), and sintered at 825 °C for 8 h under flowing 5% H_2/95% N_2 gas with a heating and cooling rate of 3 °C min^{-1}.

The products were re-ground using an agate mortar and pestle. Phase purity was confirmed by X-ray powder diffraction on a PanAnalytical X'Pert diffractometer using Cu Kα radiation (1.54183 Å) and high-energy synchrotron radiation using the 11-BM at the Advanced Photon Source (0.457868 Å). The synchrotron data were collected at 100 K. The Rietveld refinement was conducted using the GSAS software and EXPGUI interface.[28] The rare-earth occupation in the refinement was fixed due to the low substitution concentration. The final crystal structure was visualized using VESTA.[29] Scanning electron microscopy (SEM) and energy-dispersive X-ray spectroscopy (EDS) measurements were collected using a Phenom Pharos scanning electron microscope attached with a 25 mm^2 silicon drift detector (SDD) energy-dispersive X-ray spectrometer (Thermo Fisher Scientific). An accelerating voltage of 15 keV and an emission current of 12 μA were used. The powder was mounted on carbon tape, and at least five independent points of EDS analysis were analyzed on different areas of the polycrystalline sample to determine the average composition. The average particle size was determined based on an analysis of ~1500 particles.

The phase pure samples were deposited on a quartz slide (Chemglass) after being mixed in an optically transparent silicone resin (GE Silicones, RTV 615). Photoluminescent spectra were recorded on a Horiba Fluoromax-4 fluorescence spectrophotometer with a 150 W xenon arc lamp for excitation. Temperature-dependent emission spectra were obtained using a PTI fluorescence spectrophotometer with a 75 W xenon arc lamp for excitation and a Janis cryostat (VPF-100) for a temperature-controlled environment from 80 to 640 K. The internal photoluminescent quantum yield (PLQY) and external quantum efficiency (EQE) were determined following the methodology of de Mello et al. using a Spectralon-coated integrating sphere (Labsphere) with an inner diameter of 150 mm.[30] The aliovalent substitution results in defect-induced trap states, which can influence the ability to measure the PLQY accurately. Thus, the sample was heated in the dark for 5 min at 140 °C to release any trapped electrons. The PLQY measurements could then be reproducibly carried out. The same procedure was followed to determine the PLQY of commercially purchased $BaMgAl_{10}O_{17}:Eu^{2+}$. Temperature-dependent luminescent decay curves were obtained using a NanoLED N-363 nm LED coupled to a Horiba DeltaFlex Lifetime System. Fabrication of a pc-LED involved using $(Na_{1.92}Eu_{0.04})MgPO_4F$, commercially available β-$SiAlON:Eu^{2+}$ (Mitsubishi Chemical Corporation), and in-house prepared $Sr_2Si_5N_8:Eu^{2+}$. The ratio of each phosphor was optimized to 4.23 wt % $Sr_2Si_5N_8:Eu^{2+}$, 52 wt % $(Na_{1.92}Eu_{0.04})MgPO_4F$, and 2.94 wt % of β-$SiAlON:Eu^{2+}$ for the 405 nm LED device. The phosphors were weighed out in the appropriate ratios and mixed in the GE silicone resin. The phosphor "cap" was prepared by curing the phosphor resin in a

https://doi.org/10.1021/acsami.1c00909
ACS Appl. Mater. Interfaces 2021, 13, 16669−16676

custom brass mold and excited using a 405 nm LED driven by a forward bias of 20 mA. The white light spectrum of the prototype was directly compared to the spectrum of a "Soft White" Sylvania 60 W equivalent LED light bulb (A19, 8.5 W, 800 lumen, CCT = 2700 K). Both devices' luminescence spectra and performance were characterized using an Avasphere-5-IRRAD spectrophotometer and AvaSoft 8 software.

2.2. Chemical and Thermal Stability. The phosphor's stability against hydrolysis was investigated by dispersing the as-prepared powder in deionized water for 7, 14, and 21 days. A magnetic stir plate was used to continually agitate the powder in the water with a speed of 200 rpm. This same study was repeated using commercially purchased $BaMgAl_{10}O_{17}:Eu^{2+}$ ($BAM:Eu^{2+}$). The oxidation resistance of the rare-earth ion in $(Na_{1.92}Eu_{0.04})MgPO_4F$ was also investigated by annealing the phosphor at 80, 120, 160, and 300 °C for a total of 48 days. The powder X-ray diffractograms, emission spectra, SEM-EDS, and photoluminescent quantum yield of the annealed and hydrolyzed samples were collected after testing to identify any structural, chemical, or optical changes. To compare the performance of the fluorophosphate phosphor to $BAM:Eu^{2+}$, samples of commercial-grade $BAM:Eu^{2+}$ were also annealed at 120, 160, and 300 °C for 20 days. The powder X-ray diffractograms, emission spectra, and photoluminescent quantum yield were collected every 5 days.

3. RESULTS AND DISCUSSION

3.1. Synthesis and Crystallography. This compound was originally prepared as single crystals from the slow cooling of a melt of the appropriate precursors.[31] Here, $(Na_{2-2x}Eu_x)MgPO_4F$ (x = 0, 0.005, 0.01, 0.02, 0.04, and 0.06) is prepared as a polycrystalline product for the first time by sintering at 825 °C, as seen in Figure S1. The single reaction at moderate temperatures allows for easily scaled production of this material. Scanning electron microscopy (SEM) revealed irregular particle morphology and an average particle size of 8.36 μm (Figure S2a), while the energy-dispersive X-ray spectrum (EDS) (Figure S2b) and element mapping (Figure S2c) show that all of the loaded elements are present and homogeneously dispersed throughout each particle. The average composition by EDS was $Na_{1.96}MgP_{0.88}O_{4.29}F_{1.02}$, closely resembling the nominally loaded composition (Table S1). The Rietveld refinement of high-energy synchrotron X-ray powder diffraction (11-BM at APS) of $Na_{1.92}Eu_{0.04}MgPO_4F$ (Figure 2a) also shows excellent agreement with the published crystal structure. The refinement statistics are provided in Table S2, and the refined crystal structure data is provided in Tables S3.

Na_2MgPO_4F crystallizes in the orthorhombic space group *Pbcn* (No. 60). The crystal structure's rigid backbone is composed of densely connected $Na_2MgF_2O_{11}$ units (Figure 2b). This complex unit is constructed from two crystallographically independent, Na-centered, NaO_5F_2 polyhedra that are face sharing with two highly distorted MgO_4F_2 octahedra.[31] The phosphorous atoms are tetrahedrally coordinated by oxygen and sit between the clusters. The substitution of Eu^{2+} ions are expected to occur for one or both of the Na^+ ions despite being isovalent with Mg^{2+} because Eu^{2+} ($r_{6\text{-coord}}$ = 1.17 Å; $r_{7\text{-coord}}$ = 1.20 Å) is much closer in size to Na^+ ($r_{7\text{-coord}}$ = 1.12 Å) than Mg^{2+} ($r_{6\text{-coord}}$ = 0.720 Å).[32]

3.2. Photoluminescence Properties. Substituting Eu^{2+} for Na^+ following $(Na_{2-2x}Eu_x)MgPO_4F$ (x = 0.005, 0.01, 0.02, 0.04, and 0.06) yields a bright blue light easily visible using a UV flashlight. Examining the excitation spectrum indicates four

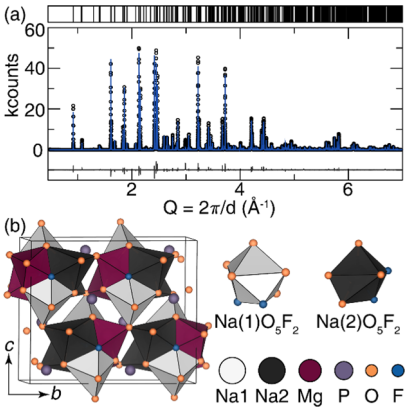

Figure 2. (a) Rietveld refinement of $Na_{1.92}Eu_{0.04}MgPO_4F$. The black circles represent the measured data, the refinement fit is in blue, and the gray line represents the difference. (b) The structure of Na_2MgPO_4F is composed of two crystallographically independent NaO_5F_2 polyhedra.

main peaks centered at approximately 275, 340, 365, and 400 nm (Figure 3a). Blue-emitting phosphors exhibiting excitation

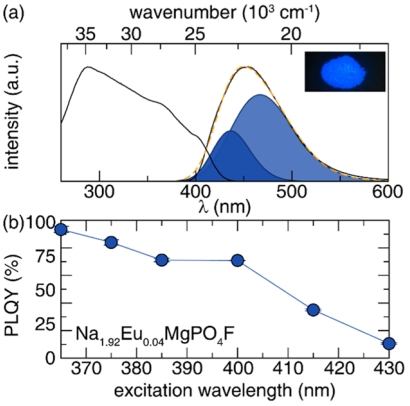

Figure 3. (a) Excitation (λ_{em} = 456 nm) and emission (λ_{ex} = 365 nm) spectra of $(Na_{1.92}Eu_{0.04})MgPO_4F$. The dashed yellow line is the fit. The inset is a photograph of the phosphor under an ultraviolet lamp (λ_{ex} = 365 nm). (b) Room-temperature PLQY of $(Na_{1.92}Eu_{0.04})MgPO_4F$ using different excitation wavelengths.

maxima at ~340 and ~365 nm are common; however, the fact that this phosphor can be excited at 400 nm and produce blue light implies a uniquely short Stokes' shift. This is particularly critical for the reduction of blue emission for human-centric warm LED lighting.[14]

Irradiating $(Na_{2-2x}Eu_x)MgPO_4F$ (x = 0.005, 0.01, 0.02, 0.04, and 0.06) at each excitation maximum yields an emission curve centered from 446 to 457 nm depending on the value of x. The observed red shift is ascribed to the incorporation of Eu^{2+}, shortening the average polyhedral bond length and enhancing the rare-earth's 5d crystal field splitting. The emission peak also broadens slightly as a function of rare-earth concentration (Figure S3). The emission curve of $(Na_{1.92}Eu_{0.04})MgPO_4F$, shown in Figure 3a, was monitored under 365 nm excitation to ensure that the entire emission curve was captured for further analysis. This emission peak can be deconvoluted into two Gaussian curves due to the simultaneous substitution of Eu^{2+} on both the Na(1) and Na(2) sites, as suggested by the crystal structure refinement data. The curves are separated by only ~1500 cm^{-1} with the integrated peak areas in an approximate 1:3 ratio. The dual substitution is further corroborated by fitting

https://doi.org/10.1021/acsami.1c00909
ACS Appl. Mater. Interfaces 2021, 13, 16669−16676

the luminescent decay curve to a biexponential, yielding lifetimes of τ_1 = 1.04 μs and τ_2 = 0.66 μs (τ_{avg} = 0.85 μs) upon 363 nm excitation. It is important to note that the shape of the decay curve and subsequent lifetime does not change after detrapping the phosphor. The observed broadening in the emission peak upon increasing Eu^{2+} concentration can thus be attributed to an increased energy transfer from the higher energy luminescent center to the lower energy luminescent center (Figure S3).[33] The 1931 CIE coordinates of $(Na_{1.92}Eu_{0.04})MgPO_4F$ under 400 nm excitation are (0.152, 0.124) and depict the deep blue emission color visually observed for this material's luminescence. The full width at half-maximum of the emission of $(Na_{1.92}Eu_{0.04})MgPO_4F$ is 79 nm (3782 cm^{-1}), which is ideal for covering the blue and cyan region of the visible region when excited by a violet LED and produces a full-spectrum white light.[22]

The room-temperature internal photoluminescent quantum yield (PLQY) of $(Na_{2-2x}Eu_x)MgPO_4F$ under 400 nm excitation was subsequently measured by following the methodology of de Mello et al. to determine the optimal Eu^{2+} concentration, maximum PLQY, and compatibility of the phosphor with a violet LED chip.[30] As plotted in Figure S4, the PLQY of $(Na_{2-2x}Eu_x)MgPO_4F$ reaches a maximum of 71.8(9)% when x = 0.04. The maximum external quantum efficiency (EQE) at this substitution concentration is 18.1(7)% (Figure S5a). Increasing the Eu^{2+} concentration causes the efficiency to drop due to concentration quenching and charge transfer from the face-sharing polyhedral environments around the luminescent centers. This PLQY surpasses $Ca_{4.98}Eu_{0.02}(PO_4)_3Cl$ (PLQY = 25%) and is similar to $(Ca_{1-x}Ce_x)_6Ba(P_{1-6x/4}Si_{6x/4})_4O_{17}$ (PLQY = 70%) but falls behind $Ca_2PO_4Cl:Eu^{2+}$ (PLQY = 84.8%) and commercially purchased $BaMgAl_{10}O_{17}:Eu^{2+}$ (PLQY = 90%) under violet excitation.[19,34,35] The PLQY and EQE of $(Na_{1.92}Eu_{0.04})MgPO_4F$ was also measured across its excitation band, spanning the near-UV and visible region, provided in Figures 3b and S5b, respectively. Under 365 nm excitation, the PLQY is 93.4(3)% and linearly decreases to 71.2(1)% under 385 nm and finally to 35.1(6)% at 415 nm. The EQE follows a similar trend with a maximum of 42.0(2)% upon 365 nm excitation that decreases to 6.1(5)% at 415 nm. The impressive efficiency of $Na_{1.92}Eu_{0.04}MgPO_4F$ when excited by violet light indicates that this phosphor is viable for device integration, especially considering post-processing techniques such as additional sintering and improved particle morphology can improve the PLQY and drastically increase the EQE.

Phosphors considered for LED-based lighting applications must also possess a thermally robust emission with chromaticity stability.[12] Indeed, LED light bulbs operate at ~423 K, which can negatively impact the shape, maximum, and intensity of the emission curve.[36] Thus, the emission spectrum of $(Na_{1.92}Eu_{0.04})MgPO_4F$ was measured from 80 to 640 K under 365 nm (Figure 4a) and 400 nm (Figure S6) excitation to determine how the emission peak changes as a function of temperature. At 80 K (blue), two emission peaks from Eu^{2+} substituting on the two Na^+ sites can be resolved. Incrementally increasing the temperature causes the higher energy peak to increase in intensity (purple) before the low energy peak begins to preferentially quench (red). A slight blue shift in the emission spectra can be observed between 100, 300, and 500 K. The blue shift is due to the combination of an increase in the intensity of the higher energy peak as a function of temperature and the preferential quenching of the low energy peak at elevated temperatures. Interestingly, the combination of blue shift and

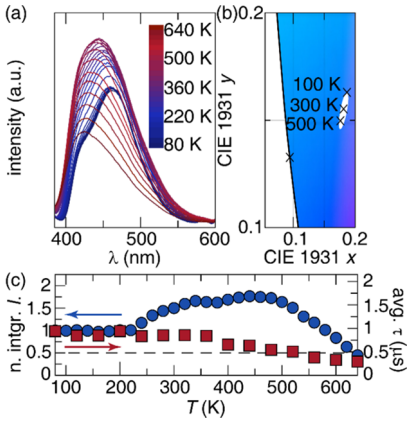

Figure 4. (a) Emission spectra from 80 K (blue) to 640 K (red) under 365 nm excitation. (b) CIE color coordinates (×) of the emission at 100, 300, and 500 K and a three-step MacAdam ellipse (white) based on the 300 K data. (c) Normalized, integrated intensity of the emission as a function of temperature (blue) and the temperature-dependent lifetime (red). The dashed line represents where the integrated emission intensity and lifetime become 50% of the 80 K value.

notable change in peak shape does not noticeably influence the CIE coordinates, as seen in Figure 3b. Analyzing the temperature-dependent color shift through a three-step MacAdam ellipse (white) based on the 300 K CIE coordinates shows that the 100 K emission spectrum falls outside the room-temperature MacAdam ellipse signifying the phosphor's color at low temperature will be distinguishable by the average human eye.[37] However, the CIE coordinates of the 500 K emission sit on the edge of the room-temperature MacAdam ellipse, indicating that there will be a just-noticeable color difference of this phosphor going from room temperature (300 K) to a device's operating temperature (500 K).[38] Moreover, the shift in chromaticity coordinates from 300 to 500 K differ less than 0.015 as required by the Enterprise Europe Network.[39] This outcome is critical because it indicates that $(Na_{1.92}Eu_{0.04})MgPO_4F$ has excellent chromaticity stability across the range of temperatures typically experienced in an LED light bulb, further enhancing the human visual experience.

A phosphor's thermal stability can be quantified by the temperature at which the emission intensity is 50% of the low-temperature intensity, called the T_{50}. The T_{50} of $(Na_{1.92}Eu_{0.04})MgPO_4F$ was first determined by plotting the normalized, integrated area of each emission peak, provided in Figure 4b. The integrated area (blue, circle) remains steady until 200 K. Increasing the temperature causes the intensity to rise, presumably due to the release of electrons from defect trap states that arise from the aliovalent substitution of Eu^{2+} for Na^+.[40] This is corroborated by temperature-dependent excitation measurements, which did not show a sufficient increase in the UV absorption as a function of temperature (Figure S7). Ultimately, this detrapping effect is beneficial and improves the thermal stability of the phosphor. The intensity reaches a maximum at 460 K, where the normalized, integrated intensity is almost double the 80 K value. Because of the dramatic detrapping in this phosphor, zero thermal quenching was observed until 580 K. It is important to note that these trap states do not induce persistent luminescence. Therefore, no residual blue light will be observed once the excitation source is turned off, minimizing exposure to blue light when integrated into an LED bulb. Quenching begins beyond 580 K where the T_{50} was

https://doi.org/10.1021/acsami.1c00909
ACS Appl. Mater. Interfaces 2021, 13, 16669−16676

determined to be 634 K. Carrying out this measurement using 400 nm excitation shows a similar optical response, including a T_{50} of 604 K (Figure S6). The ambiguity in the value of the T_{50} stems from the anomalous increase in intensity as a function of temperature. It is known that luminescent lifetime is also proportional to the internal PLQY; therefore, temperature-dependent lifetime (red, square) was also conducted to determine the T_{50}.[41] The decay curves and biexponential fits can be seen in Figure S8. The average lifetime at 80 K is 0.94 μs, meaning that the T_{50} occurs when the lifetime is 0.47 μs, approximated as the dashed line in Figure 4c. The T_{50} based on the photoluminescence lifetime was determined to be 520 K, which still surpasses the operating temperature of most LED lights (423 K). The excellent thermal stability of this phosphor makes it equally promising as a candidate for high-powered, energy-efficient LED-based lighting.

3.3. Chemical Stability and Device Integration. The harsh operating conditions experienced by a phosphor when integrated into a LED bulb can drastically affect the material's optical properties. Under prolonged operation, phosphors such as BAM:Eu^{2+} have been known to hydrolyze in the presence of moisture and lose emission intensity due to oxidation of Eu^{2+} to Eu^{3+}.[14,16,17] Therefore, the stability of $(Na_{1.92}Eu_{0.04})MgPO_4F$ against hydrolysis was investigated by dispersing the phosphor powder in deionized water for 21 days and analyzing the powder X-ray diffractograms, emission spectra, and PLQY. The powder diffractogram and EDS analysis of $(Na_{1.92}Eu_{0.04})MgPO_4F$, provided in Figure S9a and Table S4, respectively, indicate that the crystal structure is not affected by water over the entire period studied. This result is somewhat surprising considering that many oxyfluorides and fluorides, including $Sr_3(AlO_4F)$:Ce^{3+} and the popular red-emitter K_2SiF_6:Mn^{4+}, degrade upon contact with moisture.[5,42] Monitoring the emission spectrum upon 365 nm excitation (Figure S9b) reveals virtually no change in the peak shape, position, and full width at half-maximum. Conducting the same water stability tests on commercial-grade BAM:Eu^{2+} showed that the average structure does not change, although the emission peak broadens by approximately 4 nm (224 cm^{-1}) (Figure S10). This is comparable with a study done by Mishra and co-workers that showed the emission peak to broaden and red-shift by approximately 10 nm (330 cm^{-1}).[17] The quantum yield of the commercial BAM:Eu^{2+} also did not show any significant change as a result of the water exposure. Interestingly, the only observable effect of hydration on $(Na_{1.92}Eu_{0.04})MgPO_4F$ was a slight increase in the measured internal PLQY, although this still falls within the standard deviation of the measurements (Figure 5). These results ultimately indicate that the emission of $(Na_{1.92}Eu_{0.04})MgPO_4F$ is incredibly stable with respect to moisture.

Fresh samples of $(Na_{1.92}Eu_{0.04})MgPO_4F$ were also annealed in air at 80, 120, 160, and 300 °C to determine the oxidation resistance of this phosphor. The powder X-ray diffractograms and optical characteristics were collected after sitting for 1, 3, 6, 12, 24, and 48 days at elevated temperatures. The crystal structure (Figure S11) and composition (Table S5) remain relatively unaffected after prolonged heating, irrespective of the annealing temperature. Monitoring the photoluminescence under 365 and 390 nm excitation showed that the emission peak position and full width at half-maximum were nearly constant even after annealing (Figures S12 and S13). However, a closer analysis of the emission spectrum using 390 nm excitation revealed minor Eu^{3+} emission peaks that increase in intensity as a function of annealing time. The increased presence of Eu^{3+} from the oxidation of Eu^{2+} after 48 days of annealing at 80, 120, and 160 °C causes the PLQY to decrease by ~25%. Annealing at 300 °C causes a 40% decrease (Figure 5).

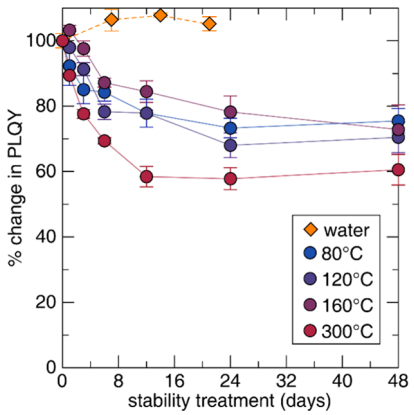

Figure 5. Percent change in the internal PLQY after 21 days of water immersion (orange diamond) and annealing at 80 °C (blue), 120 °C (purple), 160 °C (maroon), and 300 °C (red) over 48 days.

Prolonged annealing of commercial-grade BAM:Eu^{2+} has also been reported to cause rare-earth oxidation, leading to reduced emission intensity, and, more critically, a blue shift in the emission peak.[17] To compare the oxidation resistance of the fluorophosphate phosphor to present-day commercial-grade BAM:Eu^{2+}, the phosphor was annealed at 120, 160, and 300 °C. The average crystal structure and optical characteristics were monitored every 5 days. The results showed that the average structure did not change (Figure S14) and annealing BAM:Eu^{2+} up to 120 °C had little effect on the emission spectrum. Annealing at 160 and 300 °C, provided in Figure S15, caused the emission peak to broaden as a function of temperature and slightly red-shift. The most significant increase in full width at half-maximum was by 4.5 nm (205 cm^{-1}) after 20 days of annealing at 300 °C. After 20 days of annealing, the quantum yield remained robust to the oxidative environment by retaining >90% efficiency (Figure S16). The incredible oxidation resistance of commercial BAM:Eu^{2+} shows the feat of ≈15 years of industrial post-processing and material optimization. Similar techniques could be applied to $(Na_{1.92}Eu_{0.04})MgPO_4F$ to improve the fluorophosphate's chemical stability further and allow it to be utilized as the blue emitter in violet LED-driven devices for human-centric lighting.

Finally, to prove the capability of this phosphor in human-centric light bulbs, a prototype device was constructed using a violet (λ_{em} ≈ 405 nm) LED chip and a phosphor blend of the title $(Na_{1.92}Eu_{0.04})MgPO_4F$ phosphor, green-emitting β-SiAlON:Eu^{2+}, and red-emitting $Sr_2Si_5N_8$:Eu^{2+}. These data were then directly compared to a commercially available Soft White Sylvania LED light bulb (CCT = 2700 K). Figure 6a shows the full-spectrum white light from both devices. The full coverage white light spectrum from the 405 nm LED-driven device is made possible due to the broad emission band of $(Na_{1.92}Eu_{0.04})MgPO_4F$ covering the blue and cyan region of the visible spectrum. The Sylvania LED light bulb possesses a large cavity in the cyan region due to the narrow LED emission.[24] The CIE coordinates of the violet LED (square) is (0.465, 0.421), corresponding to a CCT of 2710 K, whereas the Sylvania bulb (diamond) has coordinates of (0.449, 0.405) and a CCT of 2776 K (Figure 6b). Both devices are capable of producing a warm

https://doi.org/10.1021/acsami.1c00909
ACS Appl. Mater. Interfaces 2021, 13, 16669−16676

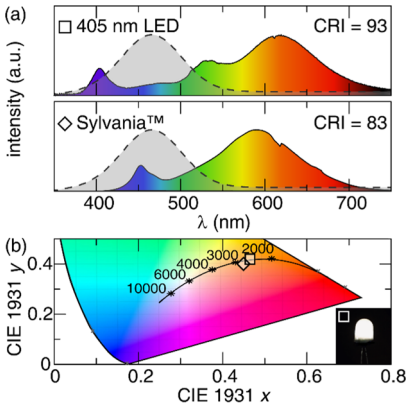

Figure 6. (a) Obtained white light spectrum of a prototype device composed of $(Na_{1.92}Eu_{0.04})MgPO_4F$, β-SiAlON:Eu^{2+}, and $Sr_2Si_5N_8$:Eu^{2+} driven by a 405 nm LED and a Soft White Sylvania LED light bulb. A wavelength-dependent melatonin suppression curve is provided for reference (gray, dashed). (b) CIE coordinates of the prototype device (square) and the Sylvania bulb (diamond). The prototype device can be seen in the inset.

white light (inset, Figure 6b); yet, the device using $(Na_{1.92}Eu_{0.04})MgPO_4F$ has a significantly higher color rendering index (CRI) of 93.4 compared to 83.4 from the Sylvania bulb. Therefore, the violet-based light allows for an improved visual experience. The luminous efficacy of radiation (LER) of the prototype is 279 lm W^{-1} compared to 359 lm W^{-1} for the Sylvania bulb, or 41 and 53%, respectively, of the ideal monochromatic (555 nm) source.[43] Considering that the device created here differs by only 12% compared to a commercial bulb supports the ability to replace 450 nm LEDS with 405 nm LEDS for warm white lighting while maintaining energy efficiency. It is important to note, however, that the LER was calculated based on the radiant flux of the source. The radiant flux is dependent upon the quality of the LED incorporated in the device and directly affects the efficacy of the light.[44] The LER is also highly influenced by the Stokes shift. As a result, 405 nm LEDs are penalized more than 450 nm LEDs due to the larger Stokes shift experienced by violet LEDs. Considering these two factors, the 12% difference in the LER of both devices is inherent from the differences in Stokes shift and may be further minimized by utilizing higher-quality LEDs in future devices.

Finally, the production of a human-centric warm white light can be analyzed through a wavelength-dependent melatonin suppression curve (dashed). The blue light intensity from the violet LED device is significantly less than the blue LED emission from the Sylvania LED light bulb. This implies that melatonin production will not be significantly disrupted using a 405 LED and Na_2MgPO_4F:Eu^{+2} in the generation of a warm white light. These results convey the capability of this prototype device in producing a white light spectrum with drastically less intense blue light without compromising on the excellent CRI and CCT required for domestic lighting by utilizing Na_2MgPO_4F:Eu^{+2} as the blue emitter in violet LED-based light bulbs.

4. CONCLUSIONS

In summary, Eu^{2+}-substituted Na_2MgPO_4F was prepared through a single-step solid-state reaction. Optical characterization indicates that Na_2MgPO_4F:Eu^{2+} can be efficiently excited by a violet LED to generate a bright blue emission with a full width at half-maximum of 79 nm (3782 cm^{-1}) and room-temperature PLQY of 71.8(9)% upon 400 nm excitation. Temperature-dependent luminescent measurements reveal trap states that delay quenching until 580 K, making the emission thermally robust. The stability of Na_2MgPO_4F:Eu^{2+} with respect to moisture and oxidation was analyzed, where the phosphor showed negligible changes after prolonged exposure to water but a 40% loss in PLQY after sitting at 300 °C for 48 days. Finally, Na_2MgPO_4F:Eu^{2+} was evaluated for human-centric lighting by fabricating a prototype device driven by a 405 nm LED. The device produced a superior warm white light (CCT = 2710 K) compared to the purchased Soft White Sylvania LED light bulb. Indeed, an exceptional color rendering index (R_a = 93) was achieved while drastically decreasing the amount of blue emission in the white light spectrum. The exceptional optical properties of the Na_2MgPO_4F:Eu^{2+} phosphor allow for the production of warm human-centric lighting, effectively transforming the future of LED-based lighting.

■ ASSOCIATED CONTENT

Supporting Information

The Supporting Information is available free of charge at https://pubs.acs.org/doi/10.1021/acsami.1c00909.

X-ray powder patterns; SEM-EDS analysis; Rietveld refinement results; quantum yield; temperature-dependent emission spectra; and chemical stability analysis (PDF)

■ AUTHOR INFORMATION

Corresponding Author

Jakoah Brgoch − *Department of Chemistry, University of Houston, Houston, Texas 77204, United States;* orcid.org/0000-0002-1406-1352; Email: jbrgoch@uh.edu

Author

Shruti Hariyani − *Department of Chemistry, University of Houston, Houston, Texas 77204, United States;* orcid.org/0000-0002-4707-8863

Complete contact information is available at: https://pubs.acs.org/10.1021/acsami.1c00909

Notes

The authors declare no competing financial interest.

■ ACKNOWLEDGMENTS

The authors would like to thank the National Science Foundation (CER-1911311) as well as the Welch Foundation (E-1981) for supporting this work. This work used the resources available through the 11-BM beamline at the Advanced Photon Source, an Office of Science User Facility operated for the U.S. Department of Energy (DOE) Office of Science by Argonne National Laboratory, under Contract No. DE-AC02-06CH11357.

■ REFERENCES

(1) Mure, L. S.; Vinberg, F.; Hanneken, A.; Panda, S. Functional Diversity of Human Intrinsically Photosensitive Retinal Ganglion Cells. *Science* **2019**, *366*, 1251−1255.

(2) Schmidt, T. M.; Chen, S.-K.; Hattar, S. Intrinsically Photosensitive Retinal Ganglion Cells: Many Subtypes, Diverse Functions. *Trends Neurosci.* **2011**, *34*, 572−580.

(3) Pust, P.; Schmidt, P. J.; Schnick, W. A Revolution in Lighting. *Nat. Mater.* **2015**, *14*, 454−458.

(4) Zhu, H.; Lin, C. C.; Luo, W.; Shu, S.; Liu, Z.; Liu, Y.; Kong, J.; Ma, E.; Cao, Y.; Liu, R.-S.; Chen, X. Highly Efficient Non-Rare-Earth Red Emitting Phosphor for Warm White Light-Emitting Diodes. *Nat. Commun.* **2014**, *5*, No. 4312.
(5) Lin, C. C.; Meijerink, A.; Liu, R.-S. Critical Red Components for Next-Generation White LEDs. *J. Phys. Chem. Lett.* **2016**, *7*, 495−503.
(6) Pust, P.; Weiler, V.; Hecht, C.; Tücks, A.; Wochnik, A. S.; Henß, A.-K.; Wiechert, D.; Scheu, C.; Schmidt, P. J.; Schnick, W. Narrow-Band Red-Emitting $Sr[LiAl_3N_4]:Eu^{2+}$ as a Next-Generation LED-Phosphor Material. *Nat. Mater.* **2014**, *13*, 891−896.
(7) Prayag, A. S.; Munch, M.; Aeschbach, D.; Chellappa, S. L.; Gronfier, C. Light Modulation of Human Clocks, Wake, and Sleep. *Clocks Sleep* **2019**, *1*, 193−208.
(8) Oh, J. H.; Yang, S. J.; Do, Y. R. Healthy, Natural, Efficient and Tunable Lighting: Four-Package White LEDs for Optimizing the Circadian Effect, Color Quality and Vision Performance. *Light: Sci. Appl.* **2014**, *3*, No. e141.
(9) Nakamura, S.; Senoh, M.; Iwasa, N.; Nagahama, Si. High-Power InGaN Single-Quantum-Well-Structure Blue and Violet Light-Emitting Diodes. *Appl. Phys. Lett.* **1995**, *67*, 1868−1870.
(10) Jüstel, T.; Nikol, H.; Ronda, C. New Developments in the Field of Luminescent Materials for Lighting and Displays. *Angew. Chem., Int. Ed.* **1998**, *37*, 3084−3103.
(11) Xie, R.-J.; Hirosaki, N.; Takeda, T. Wide Color Gamut Backlight for Liquid Crystal Displays Using Three-Band Phosphor-Converted White Light-Emitting Diodes. *Appl. Phys. Express* **2009**, *2*, No. 022401.
(12) Clark, T.; Davis, L.; Duffy, M.; Gaines, J.; Hansen, M.; Haugaard, E.; Paolini, S.; Pattison, M.; Robinson, C.; Sarraf, S.; Soer, W.; van Driel, W. *LED Luminaire Reliability: Impact of Color Shift*; Department of Energy, 2017.
(13) Xiao, Y.; Xiao, W.; Zhang, L.; Hao, Z.; Pan, G.-H.; Yang, Y.; Zhang, X.; Zhang, J. A Highly Efficient and Thermally Stable Green Phosphor $(Lu_2SrAl_4SiO_{12}:Ce^{3+})$ for Full-Spectrum White LEDs. *J. Mater. Chem. C* **2018**, *6*, 12159−12163.
(14) Piquette, A.; Bergbauer, W.; Galler, B.; Mishra, K. C. On Choosing Phosphors for Near-UV and Blue LEDs for White Light. *J. Solid State Sci. Technol.* **2016**, *5*, R3146−R3159.
(15) Duke, A. C.; Hariyani, S.; Brgoch, J. $Ba_3Y_2B_6O_{15}:Ce^{3+}$—A High Symmetry, Narrow-Emitting Blue Phosphor for Wide-Gamut White Lighting. *Chem. Mater.* **2018**, *30*, 2668−2675.
(16) Oshio, S.; Matsuoka, T.; Tanaka, S.; Kobayashi, H. Mechanism of Luminance Decrease in $BaMgAl_{10}O_{17}:Eu^{2+}$ Phosphor by Oxidation. *J. Electrochem. Soc.* **1998**, *145*, 3903−3907.
(17) Mishra, K. C.; Raukas, M.; Marking, G.; Chen, P.; Boolchand, P. Investigation of Fluorescence Degradation Mechanism of Hydrated $BaMgAl_{10}O_{17}$: Eu^{2+} Phosphor. *J. Electrochem. Soc.* **2005**, *152*, H183−H190.
(18) Qiao, J.; Ning, L.; Molokeev, M. S.; Chuang, Y.-C.; Liu, Q.; Xia, Z. Eu^{2+} Site Preferences in the Mixed Cation $K_2BaCa(PO_4)_2$ and Thermally Stable Luminescence. *J. Am. Chem. Soc.* **2018**, *140*, 9730−9736.
(19) Zheng, J.; Wu, S.; Chen, G.; Dang, S.; Zhuang, Y.; Guo, Z.; Lu, Y.; Cheng, Q.; Chen, C. Blue-Emitting $Ca_5(PO_4)_3Cl:Eu^{2+}$ Phosphor for Near-UV Pumped Light Emitting Diodes: Electronic Structures, Luminescence Properties and LED Fabrications. *J. Alloys Compd.* **2016**, *663*, 332−339.
(20) Brgoch, J.; Borg, C. K. H.; Denault, K. A.; Mikhailovsky, A.; DenBaars, S. P.; Seshadri, R. An Efficient, Thermally Stable Cerium-Based Silicate Phosphor for Solid State White Lighting. *Inorg. Chem.* **2013**, *52*, 8010−8016.
(21) Zhang, S.; Hao, Z.; Zhang, L.; Pan, G.-H.; Wu, H.; Zhang, X.; Luo, Y.; Zhang, L.; Zhao, H.; Zhang, J. Efficient Blue-Emitting Phosphor $SrLu_2O_4:Ce^{3+}$ with High Thermal Stability for Near Ultraviolet (∼400 nm) LED-Chip Based White LEDs. *Sci. Rep.* **2018**, *8*, No. 10463.
(22) Yan, C.; Liu, Z.; Zhuang, W.; Liu, R.; Xing, X.; Liu, Y.; Chen, G.; Li, Y.; Ma, X. $YScSi_4N_6C:Ce^{3+}$—A Broad Cyan-Emitting Phosphor to Weaken the Cyan Cavity in Full-Spectrum White Light-Emitting Diodes. *Inorg. Chem.* **2017**, *56*, 11087−11095.
(23) Liao, H.; Zhao, M.; Molokeev, M. S.; Liu, Q.; Xia, Z. Learning From a Mineral Structure Toward an Ultra-Narrow-Band Blue-Emitting Silicate Phosphor $RbNa_3(Li_3SiO_4)_4:Eu^{2+}$. *Angew. Chem., Int. Ed.* **2018**, *57*, 11728−11731.
(24) Zhao, M.; Liao, H.; Molokeev, M. S.; Zhou, Y.; Zhang, Q.; Liu, Q.; Xia, Z. Emerging Ultra-Narrow-Band Cyan-Emitting Phosphor for White LEDs with Enhanced Color Rendition. *Light: Sci. Appl.* **2019**, *8*, No. 38.
(25) Sun, L.; Devakumar, B.; Liang, J.; Wang, S.; Sun, Q.; Huang, X. A Broadband Cyan-Emitting $Ca_2LuZr_2(AlO_4)_3:Ce^{3+}$ Garnet Phosphor for Near-Ultraviolet-Pumped Warm-White Light-Emitting Diodes with an Improved Color Rendering Index. *J. Mater. Chem. C* **2020**, *8*, 1095−1103.
(26) Liang, J.; Devakumar, B.; Sun, L.; Wang, S.; Sun, Q.; Huang, X. Full-Visible-Spectrum Lighting Enabled by an Excellent Cyan-Emitting Garnet Phosphor. *J. Mater. Chem. C* **2020**, *8*, 4934−4943.
(27) Mansouri Tehrani, A.; Ghadbeigi, L.; Brgoch, J.; Sparks, T. D. Balancing Mechanical Properties and Sustainability in the Search for Superhard Materials. *Integr. Mater. Manuf. Innovation* **2017**, *6*, 1−8.
(28) Toby, B. H. H. EXPGUI, a Graphical User Interface for GSAS. *J. Appl. Crystallogr.* **2001**, *34*, 210−213.
(29) Momma, K.; Izumi, F. VESTA 3 for Three-Dimensional Visualization of Crystal, Volumetric, and Morphology Data. *J. Appl. Crystallogr.* **2011**, *44*, 1272−1276.
(30) de Mello, J. C.; Wittmann, H. F.; Friend, R. H. An Improved Experimental Determination of External Photoluminescence Quantum Efficiency. *Adv. Mater.* **1997**, *9*, 230−232.
(31) Swafford, S. H.; Holt, E. M. New Synthetic Approaches to Monophosphate Fluoride Ceramics: Synthesis and Structural Characterization of $Na_2Mg(PO_4)F$ and $Sr_5(PO_4)_3F$. *Solid State Sci.* **2002**, *4*, 807−812.
(32) Shannon, R. D. Revised Effective Ionic Radii and Systematic Studies of Interatomic Distances in Halides and Chalcogenides. *Acta Crystallogr., Sect. A* **1976**, *32*, 751−767.
(33) Bachmann, V.; Ronda, C.; Meijerink, A. Temperature Quenching of Yellow Ce^{3+} Luminescence in YAG:Ce. *Chem. Mater.* **2009**, *21*, 2077−2084.
(34) Komuro, N.; Mikami, M.; Shimomura, Y.; Bithell, E. G.; Cheetham, A. K. Synthesis, Structure and Optical Properties of Cerium-Doped Calcium Barium Phosphate − A Novel Blue-Green Phosphor for Solid-State Lighting. *J. Mater. Chem. C* **2015**, *3*, 204−210.
(35) Chiu, Y.-C.; Liu, W.-R.; Chang, C.-K.; Liao, C.-C.; Yeh, Y.-T.; Jang, S.-M.; Chen, T.-M. Ca_2PO_4Cl: Eu^{2+}: An Intense Near-Ultraviolet Converting Blue Phosphor for White Light-Emitting Diodes. *J. Mater. Chem.* **2010**, *20*, 1755−1758.
(36) Wei, Y.; Cao, L.; Lv, L.; Li, G.; Hao, J.; Gao, J.; Su, C.; Lin, C. C.; Jang, H. S.; Dang, P.; Lin, J. Highly Efficient Blue Emission and Superior Thermal Stability of $BaAl_{12}O_{19}:Eu^{2+}$ Phosphors Based on Highly Symmetric Crystal Structure. *Chem. Mater.* **2018**, *30*, 2389−2399.
(37) Chickering, K. D. FMC Color-Difference Formulas: Clarification Concerining Usage. *J. Opt. Soc. Am.* **1971**, *61*, 118−122.
(38) Chickering, K. D. Optimization of the MacAdam-Dodified 1965 Friele Color-Different Formula. *J. Opt. Soc. Am.* **1967**, *57*, 537−541.
(39) Ni, J.; Liu, Q.; Wan, J.; Liu, G.; Zhou, Z.; Xu, F.; Zeng, X.; Xie, R.-J. Novel Luminescent Properties and Thermal Stability of Non-Rare-Earth Ca-α-SiAlON:Mn^{2+} Phosphor. *J. Lumin.* **2018**, *202*, 514−522.
(40) Garlick, G. F. J.; Gibson, A. F. The Electron Trap Mechanism of Luminescence in Sulphide and Silicate Phosphors. *Proc. Phys. Soc.* **1948**, *60*, 574−590.
(41) Müller, M.; Jüstel, T. On the Luminescence and Energy Transfer of White Emitting $Ca_3Y_2(Si_3O_9)_2:Ce^{3+}$,$Mn^{2+}$ Phosphor. *J. Lumin.* **2014**, *155*, 398−404.
(42) George, N. C.; Denault, K. A.; Seshadri, R. Phosphors for Solid-State White Lighting. *Annu. Rev. Mater. Res.* **2013**, *43*, 481−501.
(43) Ohno, Y. In *Color Rendering and Luminous Efficacy of White LED Spectra*, Proceedings Volume 5530, Fourth International Conference on Solid State Lighting, SPIE, Denver, 2004.

https://doi.org/10.1021/acsami.1c00909
ACS Appl. Mater. Interfaces 2021, 13, 16669−16676

(44) Choudhury, A. K. R. 1 - Characteristics of Light Sources. In *Principles of Colour and Appearance Measurement*; Choudhury, A. K. R., Ed.; Woodhead Publishing, 2014; pp 1−52.

https://doi.org/10.1021/acsami.1c00909
ACS Appl. Mater. Interfaces 2021, 13, 16669−16676